IEEE Access
Multidisciplinary : Rapid Review : Open Access Journal

Received April 20, 2018, accepted May 29, 2018, date of publication June 5, 2018, date of current version July 6, 2018.

Digital Object Identifier 10.1109/ACCESS.2018.2844163

A Hybrid Model for Image Denoising Combining Modified Isotropic Diffusion Model and Modified Perona-Malik Model

NA WANG[1], YU SHANG[1], YANG CHEN[2], MIN YANG[3], QUAN ZHANG[1], YI LIU[1], AND ZHIGUO GUI[1]

[1]Shanxi Provincial Key Laboratory for Biomedical Imaging and Big Data, North University of China, Taiyuan 030051, China
[2]LIST, Key Laboratory of Computer Network and Information Integration, Ministry of Education, Southeast University, Nanjing 210096, China
[3]School of Mechanical Engineering and Automation, Beijing University of Aeronautics and Astronautics, Beijing 100191, China

Corresponding author: Zhiguo Gui (gzgtg@163.com)

This work was supported in part by the National Key Scientific Instrument and Equipment Development Project of China under Grant 2014YQ24044508, in part by the National Natural Science Foundation of China under Grant 61671413, in part by the National Key Research and Development Program of China under Grant 2016YFC0101602, in part by the Natural Science Foundation of Shanxi Province under Grant 2015011046, in part by the Shanxi Province Science Foundation for Youths under Grant 201601D021080, and in part by the Science Foundation of North University of China under Grant XJJ2016019.

ABSTRACT In this paper, a hybrid image denoising algorithm based on directional diffusion is proposed. Specifically, we developed a new noise-removal model by combining the modified isotropic diffusion model and the modified Perona–Malik (PM) model. The novel hybrid model can adapt the diffusion process along the tangential direction of edges in the original image via a new control function based on the patch similarity modulus. In addition, the patch similarity modulus is used as the new structure indicator for the modified Perona–Malik model. The feature of second-order directional derivative of edge's tangential direction allows the proposed model to reduce the aliasing and the noise around edge during edge preserving smoothing. The proposed method is thus able to efficiently preserve the edges, textures, thin lines, weak edges, and fine details, meanwhile preventing the staircase effects. Computer experiments on synthetic image and nature images demonstrate that the proposed model achieves a better performance than the conventional partial differential equations models and some recent advanced models.

INDEX TERMS Image denoising, adaptive algorithm, Perona-Malik (PM) model, isotropic diffusion (ID) model, patch similarity modulus, partial differential equations (PDEs).

I. INTRODUCTION

Image processing is powerful tool for many fields including robotic vision, facial recognition, security surveillance, artificial intelligence, and medical imaging [1]–[4]. The overall performance of image processing systems depends on the quality of the test image. However, image is inevitably corrupted by noise during acquisition and transmission. Image denoising aims to faithfully reconstruct an image from its noise corrupted observation. It tends to improve the degraded image quality for better interpretation and data extraction. Therefore, image denoising is a fundamental problem and an important process for many image processing systems [5]. Image denoising has become an attractive research topic from last decades [6]–[22]. The researchers found that partial differential equations (PDEs) have significant efficiency in the field of image denoising. Rencently, many PDE-based models for image denoising have been proposed, such as the isotropic diffusion (ID) model [8], the Perona-Malik (PM) model [9], the total variation (TV) model [10], [11] and so on. Among these models, the isotropic diffusion (ID) model proposed by Witkin [8] is a pioneer of PDE-based models for noise removal. Perona and Malik [9] introduced an efficient anisotropic diffusion model based on PDE, namely the PM model. The PM model is the initial study on anisotropic diffusion model for restoration of image. Thereafter, numerous anisotropic denoising models derived from the PM model were proposed [12]–[22]. Apart from these models, the TV model is also a successful anisotropic diffusion model based PDE for image denoising. Overall, these anisotropic diffusion models have reached a good balance between noise removal and edge preserving.

Although the above second-order PDE-based anisotropic diffusion models have a good ability to minimize noise while preserving edges, they appear to have many drawbacks such as the staircase effects. In order to reduce the drawback of transforming ramps into stairs (piecewise constant regions) [13], a lot of innovative PDE-based techniques have been proposed in recent years [12], [17]–[26]. Catté *et al.* [12] proposed a modified PM model that performs a pre-denoising using a Gaussian filter before each iteration. In [19]–[22], some researchers adopted the four-order PDEs for image denoising. Those high order models minimize the staircasing effects and generate satisfactory denoising results. Barbu *et al.* [23] proposed a general variational model for image denoising and restoration, which is based on the minimization of a convex function of the gradient under minimal growth conditions. Chao and Tsai [24] proposed a new edge-preserved smoothing method based on the PM model. In this model, the edge stopping function was combined with gray-level variance and local gradient, which can preserve edges and fine details. Prasath and Vorotnikov [25] proposed a weighted and well-balanced anisotropic diffusion. Xu *et al.* [26] introduced a semi-adaptive thresholding in the PM anisotropic diffusion filter. Yahya *et al.* [15] proposed a new denoising method (TSP model) through combination of ID model, PM model, and TV model. However, the TSP model is lack of capability in preserving thin lines, weak edges and fine details while removing noise. In recent years, many studies of hybrid denoising models [29]–[32], based on either second-order PDEs (ID model, TV model or PM model) or four-order PDEs, perform remarkably excellent in removing noise while simultaneously preserving edges. It is well known that the ID model is a linear diffusion model, the linear diffusion process can be defined by the equation $\partial u/\partial t = div(\nabla u) = \Delta u$. Where Δ is Laplacian operator and it is isotropic, i.e., the diffusion is identical in all directions. The ID model has good performance for image smoothing, but fails to preserve edges. Both PM model and TV model have good performances for edge-preserving. Nevertheless the PM model and TV model can cause staircase effects and lost the local details of the observed image. Despite the many drawbacks of the ID model, TV model and PM model, they have been widely used in image denoising. All of these models do not fully consider the directional information of the local structure and reduce diffusion amount equally in all directions around the edge, therefore these models may not effectively reduce the aliasing and the noise around edge, and may lost some edge information. Geometrically speaking, 2D image regularization may be finally seen as the sum of two orthogonal and directional 1D heat flows with different diffusion intensities [17], [33]–[37]. Directional heat flows, also named directional Laplacians [17], [37], which are particularly well designed to geometrically understand the anisotropic diffusion behavior. Note that the directional Laplacian, also named as the second order directional derivative, was widely used in the PDE-based diffusion model [14], [17], [38]–[40]. Wang *et al.* [14] proposed a modified PM (MPM) model based on directional Laplacian, which diffuses the image along the edge direction of the original image. The MPM model can reduce the staircasing effects, preserve sharp discontinuities, meanwhile removing noise at edges. Ziou and Horé [38] proposed a powerful diffusion algorithm (i.e., DPM model) that can simplify and enhance the performance of the PM model. The DPM model employed an inverse diffusivity and directional diffusion to significantly reduce aliasing around step edges and lines, meanwhile preserving uniform regions. These models control diffusion process by the function of gradient, without aim to preserve the thin lines, weak edges and fine details.

As a brief summary, with the denoising models mentioned above, it is difficult to simultaneously reduce the image noise and keep the fine details by using a single model. In order to make full use of the advantages of ID model, PM model and second order directional derivative, we improved the ID model and the PM model by using second order directional derivative, respectively. Thus, the new solution we proposed in this article is a convex combination of the modified ID model and the modified PM model. A weighting function based on patch similarity modulus is used to balance the relative weights of the modified ID model and the modified PM model. This hybrid model extracts the structure of the original image and diffuses along the edge's tangential direction of the original image. By taking the advantages from modified PM (e.g., the patch similarity modulus to serve as the structure indicator) and modified ID (e.g., the performance for removing noise and edge-preserving is concurrently improved), we realized image denosing in flat region and reducing the aliasing and the noise around edges, meanwhile preserving thin lines, weak edges, textures and fine details. Moreover, the staircase effects are substantially prevented.

The remainder of this article is organized as follows: Section II mainly reviews some widely-used PDE-based models. In Section III, the details of the proposed hybrid model are described. In Section IV, we carried out a few computer experiments to evaluate the efficiency of the proposed algorithm. The conclusion of this study is reached in Section V.

II. RELATED PREVIOUS PDE-BASED DIFUSSION MODELS

A. PM MODEL

In order to well preserve edges while removing noise, Perona and Malik proposed the anisotropic PM model based on the ID model:

$$\begin{cases} \dfrac{\partial u}{\partial t} = div\left(c\left(|\nabla u|\right)\nabla u\right) \\ u(x,y,t)|_{t=0} = u_0(x,y) \end{cases} \tag{1}$$

where $c(\cdot)$ is the diffusion coefficient. Generally, $c(\cdot)$ is a nonnegative and monotone nonincreasing function over the gradient magnitude. Accordingly, the diffusion coefficient is able to adaptively control the diffusion speed, making it possible to distinguish the edges of image and decrease the diffusion in the edge regions. The diffusion coefficient

$c(\cdot)$ satisfies such requirements in that: $c(0) = 1$ and $\lim_{|\nabla u| \to \infty} c(\cdot) = 0$. Perona and Malik suggested the following two diffusion coefficients:

$$c(|\nabla u|) = \frac{1}{1 + \frac{|\nabla u|^2}{k^2}} \tag{2}$$

$$c(|\nabla u|) = \exp\left(-\frac{|\nabla u|^2}{k^2}\right) \tag{3}$$

where the gradient threshold k plays an important role in restoring an image and determining the smoothing level. If the k value is too large, the diffusion process will oversmooth and result in a blurred image. By contrast, if the k value is too small, the diffusion process will stop smoothing in early iterations and yield a restored image that is similar to the original one [24]. The selection of gradient threshold k was discussed in [41].

However, the PM diffusion model is very sensitive to noise. When the noise intensity is large, the gradient of the noise is similar to the gradient of the edge, so the PM diffusion model cannot distinguish between the true edge of the image and the false edge caused by noise. This is the primary reason that the PM model easily generates the staircase effects. Besides, the PM model is not suitable to reduce aliasing found on edges, as mentioned in [38].

B. MPM MODEL

The MPM [14] model aimed at preserving edges and suppressing staircases simultaneously in the PM model, which was a direct generalization of the PM model using directional Laplacian. It diffuses image along the edge direction of the original image.

$$\frac{\partial u}{\partial t} = \vec{n}\nabla^T \left(c(|\nabla u|)\nabla u\right)\vec{n}^T + \alpha \cdot c(|\nabla u|)\,\Delta u \tag{4}$$

where $\vec{n}$ indicates the diffusion direction and $c(|\nabla u|) = \frac{1}{\sqrt{1+|\nabla u|}}$.

C. DPM MODEL

The DPM Model [38] exploited the local curvature of pixels around edges to efficiently reduce edge aliasing while preserving the uniform regions and it can be seen as both a simplification and an enhancement of the diffusion equation of PM model.

$$\begin{cases} \dfrac{\partial u}{\partial t} = [1 - c(|\nabla u|)]\,\kappa\,|\nabla u| \\ u(x, y, t)\,|_{t=0} = u_0(x, y) + \alpha \Delta u_0(x, y) \end{cases} \tag{5}$$

where κ is the curvature along the underlying edge.

III. NEW MODEL

A. THE PROPOSED HYBRID MODEL

Image denoising aims to remove noise and preserve edges. The major denoising behavior is to reduce the degree of sharp transitions in a distorted image [25], [42]–[45]. It is generally known that noise is the high frequency components of the distorted image, and some significant high frequency components also exist around edges and textures [46], so some textures and fine details will be removed during the denoising process. In order to overcome this issue, a novel hybrid denoising model based on second order directional derivative is proposed by us in this section, namely the DLHPDE model. It combined the advantages of ID model, PM model and second order directional derivative. Additionally, we selected the patch similarity modulus as the new structure indicator in the proposed model. We used the patch similarity idea described in [47]–[50] to quantify the patch similarity modulus between neighboring patches. Let $P_{x,y}$ and $P_{x',y'}$ be the two patches centered at pixel $u_{x,y}$ (located at (x, y) on the image u) and its neighbor pixel $u_{x',y'}$ (located at (x', y') on the image u). The two patches can be described as:

$$\begin{aligned} P_{x,y} &= \left(u_{x-q,y-q}, \ldots, u_{x,y}, \ldots u_{x+q,y+q}\right)^T \\ P_{x',y'} &= \left(u_{x'-q,y'-q}, \ldots, u_{x',y'}, \ldots, u_{x'+q,y'+q}\right)^T \end{aligned} \tag{6}$$

then the patch similarity modulus between $P_{x,y}$ and $P_{x',y'}$ is calculated as follows:

$$d\left(P_{x,y}, P_{x',y'}\right) = \frac{1}{p^2}\left(\sum_{m=1}^{p^2}\left(P_{x,y}(m) - P_{x',y'}(m)\right)^2\right)^{1/2} \tag{7}$$

where the size of patch is $p \times p(p = 2q + 1)$ and q is set to 1, the $P_{x,y}(m)$ represents the m_{th} element of $P_{x,y}$ and the $P_{x',y'}(m)$ represents the m_{th} element of $P_{x',y'}$. The image patch can effectively and accurately represent the structure information. Therefore, the new structure indicator based on patch similarity modulus can identify not only the strong edges, weak edges or textures, but also the noise.

The initial form of the proposed model can be expressed as:

$$\frac{\partial u}{\partial t} = \theta \Delta u + (1 - \theta)\,\nabla\left(c\left(d\left(P_{x,y}, P_{x',y'}\right)\right)\nabla u\right) \tag{8}$$

where $\theta \in [0, 1]$ is the weighting function, patch similarity modulus $d\left(P_{x,y}, P_{x',y'}\right)$ is the structure indicator.

To better preserve edges and reduce the aliasing and the noise around edges, we employed the second order directional derivative [14], [17], [38]–[40] to modify our proposed model. Since the second order directional derivative [14], [17], [37] may be written as:

$$\frac{\partial u}{\partial t} = \vec{n}\nabla^T \nabla u \vec{n}^T \tag{9}$$

where $\vec{n}$ is a unit vector, T is the transposition, and $H = \nabla^T \nabla u$ is the Hessian matrix. The defined expression $\vec{n}H\vec{n}^T$ is the second order directional derivative of the image $u(x, y)$ along a given vector $\vec{n}$. So the proposed model can be further rewritten as follows:

$$\begin{cases} \dfrac{\partial u}{\partial t} = \theta \vec{n}\nabla^T \nabla u \vec{n}^T + (1 - \theta)\,\vec{n}\nabla^T \\ \qquad \times \left(c\left(d\left(P_{x,y}, P_{x',y'}\right)\right)\nabla u\right)\vec{n}^T \\ u(x, y, 0) = f(x, y) \\ \left.\dfrac{\partial u}{\partial N}\right|_{(x,y)\in\partial\Omega} = 0, \quad \forall t > 0 \end{cases} \tag{10}$$

where Ω is the support of the noisy image $f(x, y)$, $\partial\Omega$ is the boundary of the image $u_0(x, y)$, N is an unit outward normal to $\partial\Omega$.

Here

$$\theta = \frac{1}{1+\alpha * \sum_{P_{x',y'}\in\delta} \left(d\left(P_{x,y}, P_{x',y'}\right)\right)^2} \tag{11}$$

$$c\left(d\left(P_{x,y}, P_{x',y'}\right)\right) = \frac{k^2}{k^2+\left(d\left(P_{x,y}, P_{x',y'}\right)\right)^2} \tag{12}$$

where α is a small parameter, δ represents the neighboring patches of $P_{x,y}$ and these patches centered at the four neighbors of pixel $u_{x,y}$, k is the patch similarity modulus threshold.

To further analyze the proposed model, the Eq.(10) can be expanded as:

$$\begin{aligned}\frac{\partial u}{\partial t} &= \theta\vec{n}\nabla^T\nabla u\vec{n}^T + (1-\theta)\vec{n}\nabla^T\left(c\left(d\left(P_{x,y}, P_{x',y'}\right)\right)\nabla u\right)\vec{n}^T \\ &= \theta\vec{n}\nabla^T\nabla u\vec{n}^T \\ &\quad + (1-\theta)\left[c(\cdot)\vec{n}\nabla^T\nabla u\vec{n}^T + \vec{n}\nabla^T c(\cdot)\nabla u\vec{n}^T\right] \\ &= \theta\vec{n}\nabla^T\nabla u\vec{n}^T \\ &\quad + (1-\theta)\left[c(\cdot)\vec{n}\nabla^T\nabla u\vec{n}^T + (\nabla c(\cdot)\cdot\vec{n})(\nabla u\cdot\vec{n})\right]\end{aligned} \tag{13}$$

Note that the proposed anistropic model diffuses the image along directional vector $\vec{n}$, thus the selection of $\vec{n}$ is a key task. Generally, the gradient direction and edge direction of image are the two important options for directional vector $\vec{n}$:

- Gradient direction

$\vec{n} = \frac{\nabla u}{|\nabla u|} = \frac{(u_x, u_y)}{|\nabla u|}$, the Eq.(13) can be simplified as:

$$\begin{aligned}\frac{\partial u}{\partial t} &= \theta\vec{n}\nabla^T\nabla u\vec{n}^T \\ &\quad + (1-\theta)\left[c(\cdot)\vec{n}\nabla^T\nabla u\vec{n}^T + (\nabla c(\cdot)\cdot\vec{n})(\nabla u\cdot\vec{n})\right] \\ &= \left(\theta + c(\cdot) - \theta c(\cdot) + c'(\cdot)|\nabla u| - \theta c'(\cdot)|\nabla u|\right)u_{NN}\end{aligned} \tag{14}$$

where $u_{NN} = \frac{u_{xx}u_x^2+u_{yy}u_y^2+2u_xu_yu_{xy}}{u_x^2+u_y^2}$ is the second order derivative of image $u(x, y)$ along the gradient direction of the edges. Therefore, the diffusion is performed along the gradient direction, and the proposed model leads to the blurring of the edge structures of the image $u(x, y)$. So the directional vector of gradient direction is not the ideal choice.

- Edge direction

$\vec{n} = \frac{(\nabla u)^\perp}{|\nabla u|} = \frac{(-u_y, u_x)}{|\nabla u|}$, the Eq.(13) can be simplified as:

$$\begin{aligned}\frac{\partial u}{\partial t} &= \theta\vec{n}\nabla^T\nabla u\vec{n}^T \\ &\quad + (1-\theta)\left[c(\cdot)\vec{n}\nabla^T\nabla u\vec{n}^T + (\nabla c(\cdot)\cdot\vec{n})(\nabla u\cdot\vec{n})\right] \\ &= (\theta + c(\cdot) - \theta c(\cdot))u_{TT}\end{aligned} \tag{15}$$

where $u_{TT} = \frac{u_{xx}u_y^2+u_{yy}u_x^2-2u_xu_yu_{xy}}{u_x^2+u_y^2}$ is the second order derivative of image $u(x, y)$ along the edge direction. Therefore, the diffusion is performed along the edge direction, and the proposed model can effectively preserve edges of the image $u(x, y)$, but it also generates the staircase effects.

Inspired by the discussion in [35], the PM model can be decomposed into two terms, which expounded the PM model performs anisotropic diffusion along two orthogonal directions (gradient direction and edge direction) with different weights. And the directional diffusion term of edge direction should be encouraged since it represents a well posed smoothing operator that tend to preserve edges. Thus it is an effective denoising way to diffuse an image along the edge direction [14], [35], [38]. So the second order directional derivative of edge direction were used in our proposed model. To extract the structure of the original image (i.e., noisy image f), and to make the proposed model diffuses along the edge's tangential direction of the original image, a new directional vector is defined as $\vec{n} = \left(n_x, n_y\right) = \frac{(-f_y, f_x)}{|\nabla f|}$ in this paper. With use of the new directional vector, the final form of the proposed DLHPDE model can be rewritten as:

$$\begin{aligned}\frac{\partial u}{\partial t} &= \theta\vec{n}\nabla^T\nabla u\vec{n}^T + (1-\theta)\vec{n}\nabla^T\left(c\left(d\left(P_{x,y}, P_{x',y'}\right)\right)\nabla u\right)\vec{n}^T \\ &= \theta u_{fTT} + (1-\theta)\left(c\left(d\left(P_{x,y}, P_{x',y'}\right)\right)u_{fTT}\right. \\ &\quad \left. + \left(\nabla c\left(d\left(P_{x,y}, P_{x',y'}\right)\right)\cdot\vec{n}\right)(\nabla u\cdot\vec{n})\right)\end{aligned} \tag{16}$$

where $u_{fTT} = \frac{u_{xx}f_y^2+u_{yy}f_x^2-2f_xf_yu_{xy}}{f_x^2+f_y^2}$ is the second order derivative of image $u(x, y)$ along the edge direction of original image $f(x, y)$.

To sum up, the proposed DLHPDE model enjoy the advantages of both the modified ID model and the modified PM model. According to the value of θ, we can adaptively control the diffusion mode. For the edges and textures, the weighting function θ is close to zero, the DLHPDE model will highlight the possibility of the modified PM model. The modified PM model have better performance in preserving the edges and fine details than the PM model. For the noisy points, the weighting function θ is close to 1, the DLHPDE model will highlight the possibility of the modified ID model. The modified ID model can preserve more edges than the ID model. Note that the modified ID model and the modified PM model smooth the image $u(x, y)$ along the edge direction of image $f(x, y)$, and they can preserve the edges of the image $f(x, y)$. The structure information of original image $f(x, y)$ determines the structure property of image $u(x, y)$, so that there is neither false edge (i.e., staircase effect) in image $f(x, y)$ nor false edge in image $u(x, y)$. On the basis of these analyses, the success of the DLHPDE model is attributed to the combination of θ, $c\left(d\left(P_{x,y}, P_{x',y'}\right)\right)$, PDE based on directional diffusion, and the edge vector. By combining the merits of these elements, the DLHPDE model can efficiently preserve the edges, textures, thin lines, weak edges and fine details, and avoid the staircase effects. In addition, the DLHPDE model can reduce the aliasing and the noise around edges.

B. NUMBERICAL IMPLEMENTATION

Similar to the MPM model, in order to numerically solve the Eq.(16) of the proposed DLHPDE model by using the finite difference method, let

$$\begin{aligned} I &= \vec{n}\nabla^T \nabla u \vec{n}^T \\ &= (n_x, n_y)\begin{pmatrix} u_{xx} & u_{xy} \\ u_{xy} & u_{yy} \end{pmatrix}\begin{pmatrix} n_x \\ n_y \end{pmatrix} \\ &= u_{xx}n_x^2 + u_{yy}n_y^2 + 2u_{xy}n_x n_y \end{aligned} \tag{17}$$

$$\begin{aligned} Q &= \vec{n}\nabla^T \left(c\left(d\left(P_{x,y}, P_{x',y'}\right)\right)\nabla u\right)\vec{n}^T \\ &= (n_x, n_y)\begin{pmatrix} (c(\cdot)u_x)_x & (c(\cdot)u_y)_x \\ (c(\cdot)u_x)_y & (c(\cdot)u_y)_y \end{pmatrix}\begin{pmatrix} n_x \\ n_y \end{pmatrix} \\ &= \left[(c(\cdot)u_x)_x n_x^2 + (c(\cdot)u_y)_y n_y^2\right] + \left[(c(\cdot)u_y)_x + (c(\cdot)u_x)_y\right] n_x n_y \end{aligned} \tag{18}$$

By using Euler's forward method, the proposed DLHPDE model can be written as:

$$u_{i,j}^{r+1} = u_{i,j}^r + \Delta t\left(\theta_{i,j}^r I_{i,j}^r + \left(1-\theta_{i,j}^r\right) Q_{i,j}^r\right) \tag{19}$$

with symmetric boundary conditions:

$$\begin{aligned} &u_{-1,j}^r = u_{0,j}^r, \quad u_{M+1,j}^r = u_{M,j}^r, \quad j = 0, 1, \ldots, N \\ &u_{i,-1}^r = u_{i,0}^r, \quad u_{i,N+1}^r = u_{i,N}^r, \quad i = 0, 1, \ldots, M \end{aligned} \tag{20}$$

where $r = 0, 1, 2\ldots$ is the time level, $M \times N$ is the image size, the space grid size is set as $\Delta x = \Delta y = 1$ and the time step is set as Δt. $\theta_{i,j}^r$, $I_{i,j}^r$, $Q_{i,j}^r$ are implemented respectively according to:

$$\theta_{i,j}^r = \frac{1}{1 + \alpha * \sum\limits_{P_{i',j'} \in \delta} \left(d\left(P_{i,j}, P_{i',j'}\right)\right)^2} \tag{21}$$

$$I_{i,j}^r = D_{xx}\left(u_{i,j}^r\right) n_{xi,j}^2 + D_{yy}\left(u_{i,j}^r\right) n_{yi,j}^2 + 2 * D_{xy}\left(u_{i,j}^r\right) n_{xi,j} n_{yi,j} \tag{22}$$

$$\begin{aligned} Q_{i,j}^r = &\left[c_{Wi,j}^r\left(d\left(P_{i-1,j}^r, P_{i,j}^r\right)\right)\cdot \nabla_W u_{i,j}^r \right.\\ &\left. + c_{Ei,j}^r\left(d\left(P_{i+1,j}^r, P_{i,j}^r\right)\right)\cdot \nabla_E u_{i,j}^r\right]\cdot n_{xi,j}^2 \\ &+\left[c_{Ni,j}^r\left(d\left(P_{i,j-1}^r, P_{i,j}^r\right)\right)\cdot \nabla_N u_{i,j}^r \right.\\ &\left. + c_{Si,j}^r\left(d\left(P_{i,j+1}^r, P_{i,j}^r\right)\right)\cdot \nabla_S u_{i,j}^r\right]\cdot n_{yi,j}^2 \\ &+\left[D_x^+\left(c_{i,j}^r\left(d\left(P_{i,j+1}^r, P_{i,j-1}^r\right)\right) D_y^c u_{i,j}^r\right)\right.\\ &\left. + D_y^+\left(c_{i,j}^r\left(d\left(P_{i+1,j}^r, P_{i-1,j}^r\right)\right) D_x^c u_{i,j}^r\right)\right]\cdot n_{xi,j} n_{yi,j} \end{aligned} \tag{23}$$

where

$$d\left(P_{i-1,j}^r, P_{i,j}^r\right) = \frac{1}{p^2}\left(\sum_{m=1}^{p^2}\left(P_{i-1,j}(m) - P_{i,j}(m)\right)^2\right)^{1/2}$$

$$d\left(P_{i+1,j}^r, P_{i,j}^r\right) = \frac{1}{p^2}\left(\sum_{m=1}^{p^2}\left(P_{i+1,j}(m) - P_{i,j}(m)\right)^2\right)^{1/2}$$

$$d\left(P_{i,j-1}^r, P_{i,j}^r\right) = \frac{1}{p^2}\left(\sum_{m=1}^{p^2}\left(P_{i,j-1}(m) - P_{i,j}(m)\right)^2\right)^{1/2}$$

$$d\left(P_{i,j+1}^r, P_{i,j}^r\right) = \frac{1}{p^2}\left(\sum_{m=1}^{p^2}\left(P_{i,j+1}(m) - P_{i,j}(m)\right)^2\right)^{1/2}$$

$$\begin{aligned} D_{xx}u_{i,j}^r &= u_{i+1,j}^r + u_{i-1,j}^r - 2u_{i,j}^r \\ D_{yy}u_{i,j}^r &= u_{i,j+1}^r + u_{i,j-1}^r - 2u_{i,j}^r \\ D_{xy}u_{i,j}^r &= \frac{1}{4}\left(u_{i+1,j+1}^r + u_{i-1,j-1}^r - u_{i-1,j+1}^r - u_{i+1,j-1}^r\right) \\ \nabla_W u_{i,j}^r &= u_{i-1,j}^r - u_{i,j}^r \\ \nabla_E u_{i,j}^r &= u_{i+1,j}^r - u_{i,j}^r \\ \nabla_N u_{i,j}^r &= u_{i,j-1}^r - u_{i,j}^r \\ \nabla_S u_{i,j}^r &= u_{i,j+1}^r - u_{i,j}^r \end{aligned}$$

$$c_{Wi,j}^r\left(d\left(P_{i-1,j}^r, P_{i,j}^r\right)\right) = \frac{k^2}{k^2 + \left(d\left(P_{i-1,j}^r, P_{i,j}^r\right)\right)^2}$$

$$c_{Ei,j}^r\left(d\left(P_{i+1,j}^r, P_{i,j}^r\right)\right) = \frac{k^2}{k^2 + \left(d\left(P_{i+1,j}^r, P_{i,j}^r\right)\right)^2}$$

$$c_{Ni,j}^r\left(d\left(P_{i,j-1}^r, P_{i,j}^r\right)\right) = \frac{k^2}{k^2 + \left(d\left(P_{i,j-1}^r, P_{i,j}^r\right)\right)^2}$$

$$c_{Si,j}^r\left(d\left(P_{i,j+1}^r, P_{i,j}^r\right)\right) = \frac{k^2}{k^2 + d\left(P_{i,j+1}^r, P_{i,j}^r\right)^2}$$

and these differential operators D_x^c, D_y^c, D_x^+, D_y^+ are defined as:

$$\begin{aligned} D_x^c g_{i,j}^r &= \frac{g_{i+1,j}^r - g_{i-1,j}^r}{2} \\ D_y^c g_{i,j}^r &= \frac{g_{i,j+1}^r - g_{i,j-1}^r}{2} \\ D_x^+ g_{i,j}^r &= g_{i+1,j}^r - g_{i,j}^r \\ D_y^+ g_{i,j}^r &= g_{i,j+1}^r - g_{i,j}^r \end{aligned}$$

The flow chart in Figure 1 shows the algorithm of the proposed DLHPDE model that is applied to each pixel. The proposed algorithm can adaptively select the diffusion mode from the modified ID model and the modified PM model. When the weighting function θ is close to 1, the modified ID model will be chosen to dispose pixel, yielding a better smoothing effect. On the contrary, when the weight function θ is close to zero, the modified PM model will be chosen to dispose pixel, aiming to preserves edge.

IV. COMPUTER EXPERIMENT AND DISCUSSION

In this section, some simulation results are presented to illustrate the merit and efficiency of the proposed DLHPDE model in image denoising. All the simulation experiments are implemented by MATLAB R2008a and performed on 32-bit Windows 7 system on the desktop computer with Inter(R) Core(TM) i7-4770K CPU and 8GB RAM. Image quality

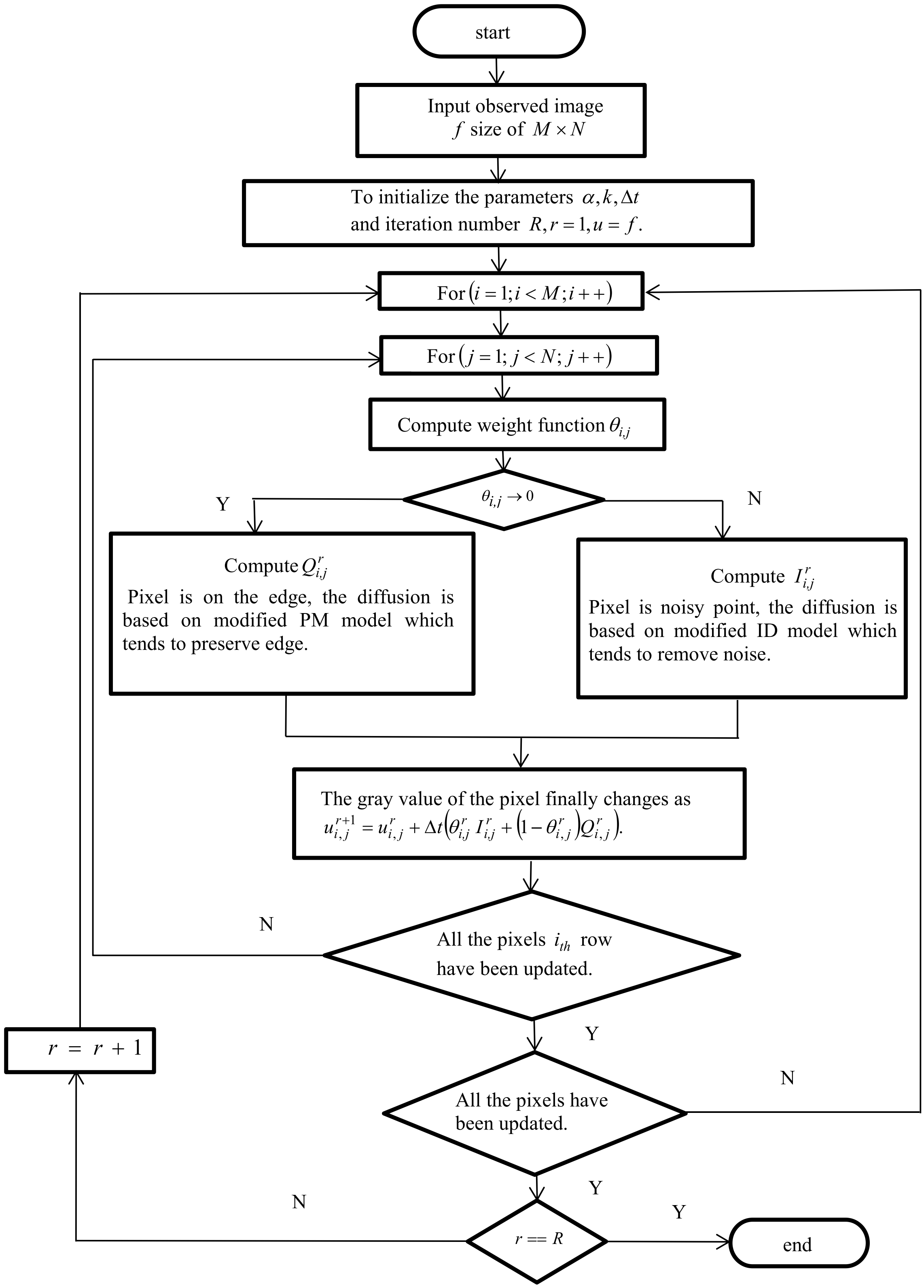

FIGURE 1. **Flow chart of the proposed DLPDE algorithm.**

assessment can be subdivided into subjective evaluation and objective evaluation. Subjective evaluation costs too much time and effort in the whole procedure. More importantly, it is impractical to perform subjective image quality assessment in real-time. Hence, the objective quality metrics that can automatically evaluate the image perceptual quality and guide

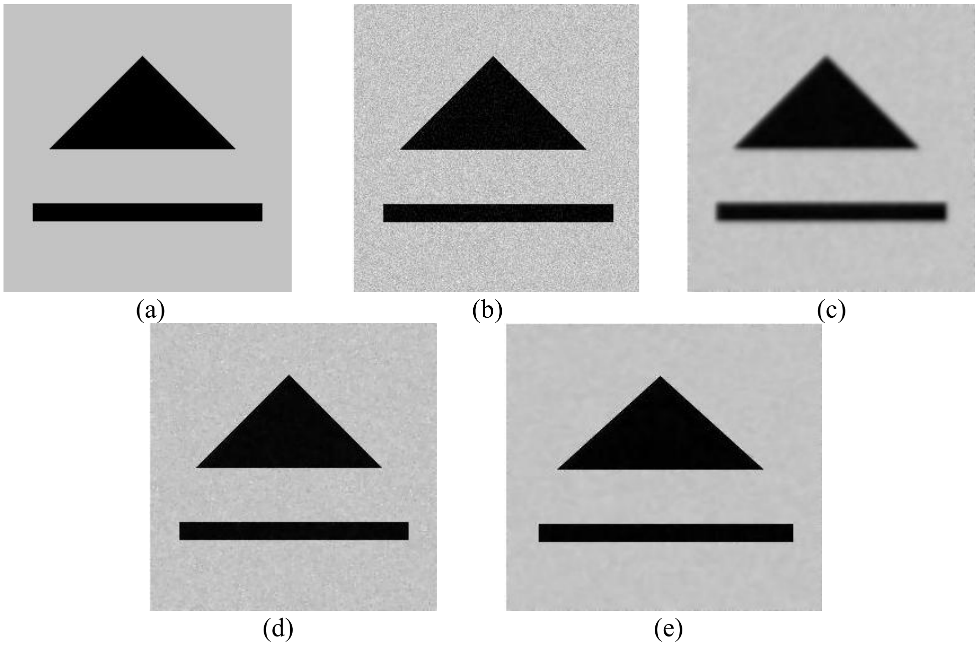

FIGURE 2. Denoising outcomes from the synthetic image(256×256). (a) clear image; (b) noisy image; (c) denoising by ID model; (d) denoising byPM model ($k = 6$); (e) denoising by DLHPDE model ($k = 2$). The iteration number is set to 12.

the image processing applications are demanded [51]. Peak signal to noise ratio (PSNR) and mean structural similarity index measure (MSSIM) [52] are widely used as the metrics in image analysis. However, the PSNR and MSSIM are two highly relevant quality measures and the PSNR is more sensitive to additive Gaussian white noise than the MSSIM [53]. So we only employed the PSNR to objectively assess the quality of restored image. The PSNR is defined as:

$$PSNR = 10\log_{10}\left(\frac{255^2 \times M \times N}{\sum_{i=1}^{M}\sum_{j=1}^{N}\left[u_{img}(i,j) - u(i,j)\right]^2}\right) \tag{24}$$

here $M \times N$ is the size of images, u_{img} and u are the true image and restored image, respectively. Generally, the larger value of the PSNR indicates the better quality of the restored image.

A. QUALITATIVE COMPARISON WITH SOME PDE-BASED MODELS

In this subsection, we compared the restored results with ID model [8], PM model [9], VEPM model [13], MPM model [14], and TSP model [15], respectively.

For comparison, the optimal parameters of ID model, PM model, VEPM model, MPM model, and TSP model in [8], [9], and [13]–[15] were selected from [14]. And all the parameters adopted for the proposed DLHPDE model are optimized in order to obtain the best quality of the restored image. The relevant parameters are set as $\alpha = 0.08$ and k varies from 1 to 30. Each denoising method will be terminated when the PSNR reached maximum, and the time step were set as $\Delta t = 0.25$ in all experiments.

We first carried out the denoising of a synthetic image to verify the performance of the proposed DLHPDE model. Figure 2 displays the different denoising results of the synthetic image. Figure 2(a) is the clear image containing a rectangle and a triangle. Figure 2(b) is the image with white Gaussian noise at zero mean and 0.003 variance. Figure 2(c) and Figure 2(d) show that the denoising results of the ID model and PM model. It is clearly that the ID model smoothed the sharp corners and the PM model generates staircases. Figure 2(e) shows that the proposed DLHPDE model performs better than the single-alone ID model and single-alone PM model. This model can also prevent the staircase effects and preserve the edges.

To further validate the performance of the proposed DLHPDE model, we performed a series of experiments on four standard testing images. These images, including Lena, Barbara, Boat and Peppers, are all in size of 256×256. The noisy images were created through adding zero-mean white Gaussian noises with different variances. As the first comparison, desnoising results of Lena image with different levels of noise are showed in Figures 3 and 5. It can be seen that the ID model blurs the edges, the PM model suffers from obvious block effects. It is clearly that, the VEPM model, MPM model and TSP model work very well on preserving the edges and smoothing the noise. However, the fine details of Lena's hair, eyes, lips are smoothed out, and slight staircase effects appear when the noise level is high. Figure 3(h) and Figure 5(h) present the restored image from the proposed

FIGURE 3. Comparison of denoising results on Lena image. (a) noise free image; (b) noisy image with variance of 0.002; Denoising results by (c) ID model, (d) PM model ($k = 6$), (e) VEPM model ($k = 4$), (f) MPM model, (g) TSP model ($k = 5$), as well as (h) DLHPDE model ($k = 2$).

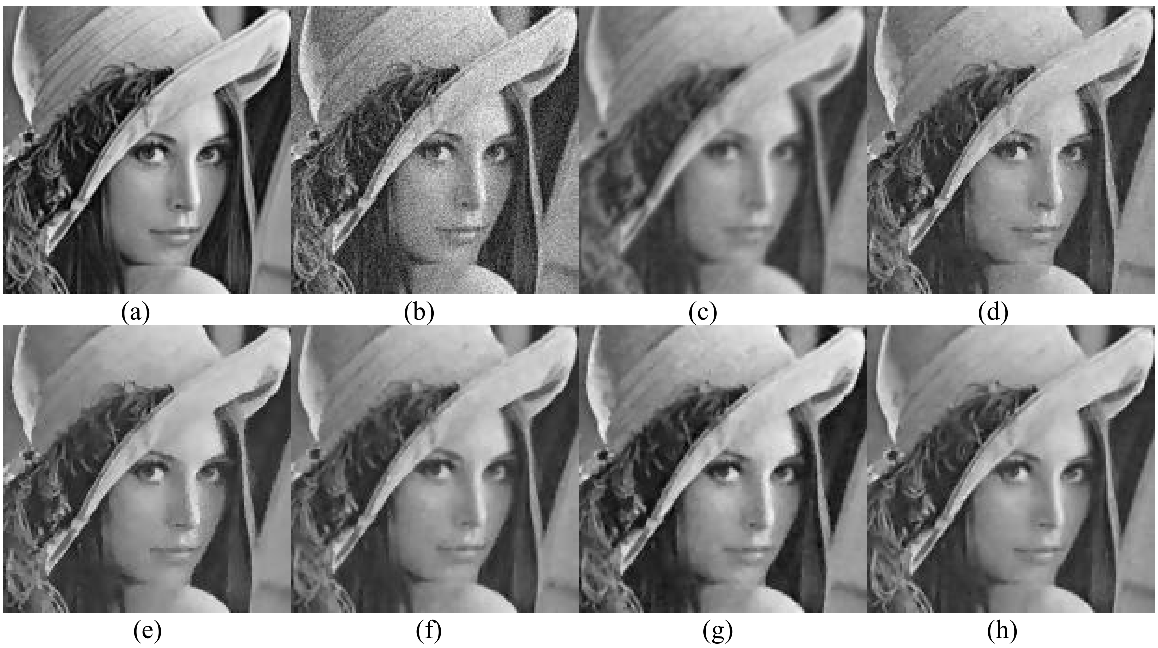

FIGURE 4. Comparison of denoising results for zoomed-in region of the Lena image. (a) noise free image; (b) noisy image with variance of 0.002; Denoising results by (c) ID model, (d) PM model ($k = 6$), (e) VEPM model ($k = 4$), (f) MPM model, (g) TSP model ($k = 5$), as well as (h) DLHPDE model ($k = 2$).

DLHPDE model. Apparently the DLHPDE model can effectively preserves the fine details while removing noise in the image. For a local region comparison, we zoomed in Lena image, from Figure 4 we can judge that the DLHPDE model provides more natural effect with clearer details. As can be seen, the PM model generates isolated points. The VEPM model and TSP model generate a small degree of staircase effects and lost fine details. The edges in MPM are sharp, but it still lost fine details. It is clearly seen that the proposed DLHPDE model substantially reduces the

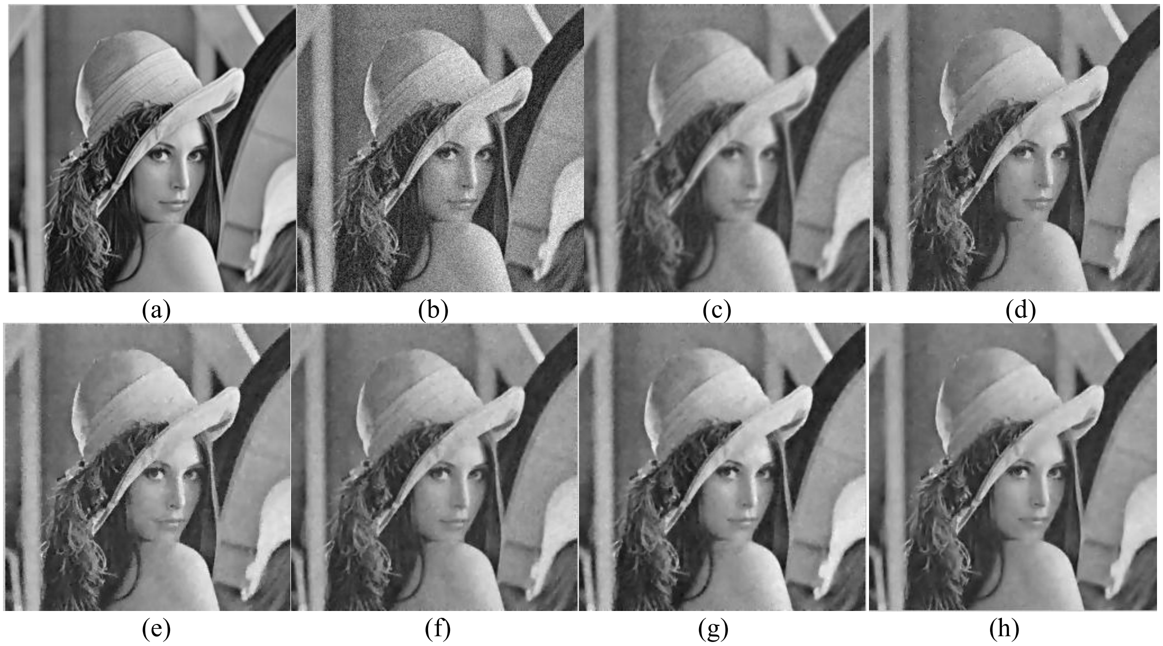

FIGURE 5. Comparison of denoising resultson Lena image. (a) noise free image; (b) noisy image with variance of 0.003; Denoising results by (c) ID model, (d) PM model ($k = 6$), (e) VEPM model ($k = 4$), (f) MPM model, (g) TSP model ($k = 5$), as well as (h) DLHPDE model ($k = 2$).

TABLE 1. Quantitative comparison of AGORITHMS IN DENOSING Lena image.

Model	Noise variance=0.002	Noise variance=0.003	Noise variance=0.005
	PSNR	PSNR	PSNR
ID	27.49	27.33	26.08
PM	31.54	30.38	28.89
VEPM	31.91	30.81	29.24
MPM	32.08	31.18	29.86
TSP	32.12	31.09	29.42
DLHPDE	**33.16**	**31.88**	**30.36**

TABLE 2. Quantitative comparison of AGORITHMS IN DENOSING Barbara image and Boat image

Image	Barbara						Boat					
	ID	PM	VEPM	MPM	TSP	DLHPDE	ID	PM	VEPM	MPM	TSP	DLHPDE
PSNR	24.18	30.00	29.75	30.08	29.14	**31.05**	27.25	31.25	31.29	31.80	31.55	**32.20**

staircase effects and the aliasing around edges and obviously preserves the edges, textures, thin lines, weak edges and fine details. The quantitative comparison results of each model are summarized in Table 1. The noisy images are corrupted by zero-mean Gaussian noise at variance of 0.002, 0.003, 0.005, respectively. The Barbara and Boat images are shown in Figures 6 and 7 respectively, and the test images are corrupted by zero-mean Gaussian noise at variance of 0.002. From Figure 6(c), it is clearly seen that the ID model removes the noises, but blurs the edges and texture regions. From Figure 6(d) to Figure 6(g), we observe that the PM model, VEPM model, MPM model, and TSP model can preserve edges and texture regions effectively, but failed to remove the noise in the texture regions. Figure 6(h) shows that the DHLPDE model can remove the noise along edges and preserve the details information of the edges and texture regions. Figure 7 shows the image outcomes processed by our proposed DLHPDE model and other five models. With DLHPDE model, the aliasing around edges are vanished and the thin lines and weak edges are well preserves.

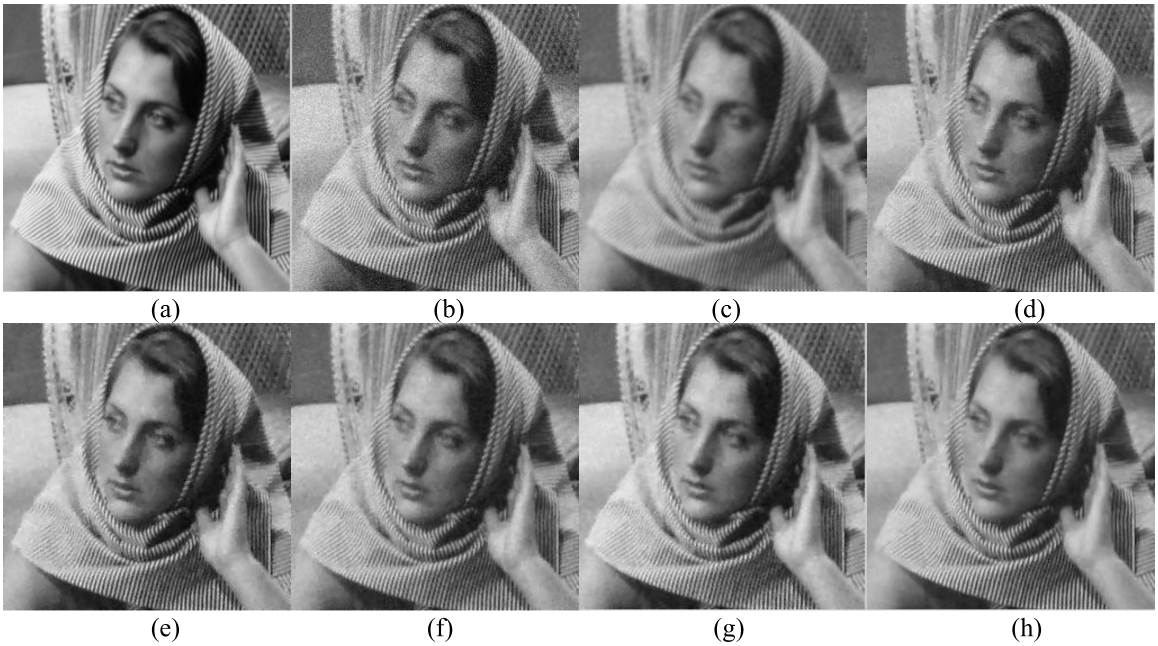

FIGURE 6. Comparison of denoising resultson Barbara image. (a) noise free image; (b) noisy image with variance of 0.002; Denoising results by (c) ID model, (d) PM model ($k = 6$), (e) VEPM model ($k = 4$), (f) MPM model, (g) TSP model ($k = 5$), as well as (h) DLHPDE model ($k = 2$).

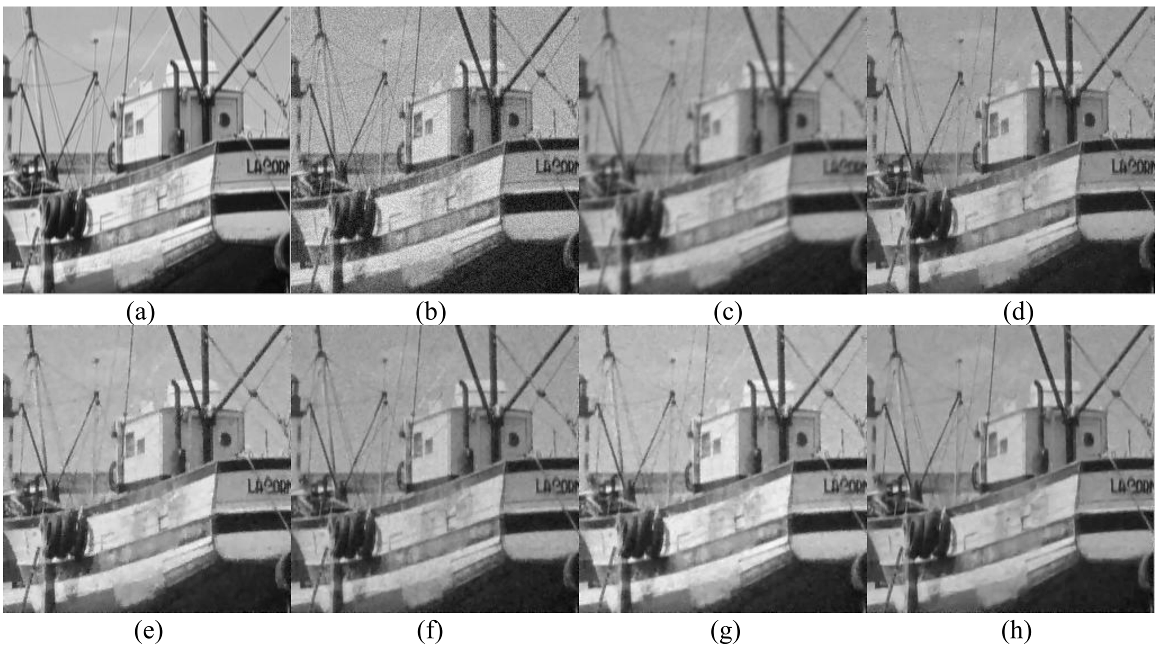

FIGURE 7. Comparison of denoising resultson Boat image. (a) noise free image; (b) noisy image with variance of 0.002; Denoising results by (c) ID model, (d) PM model ($k = 6$), (e) VEPM model ($k = 4$), (f) MPM model, (g) TSP model ($k = 5$), as well as (h) DLHPDE model ($k = 2$).

Among all the methods being compared, the DLHPDE model has the best denoising performance as well as the capability to preserve weak edges and fine details. Table 2 summarizes the quantitative comparison of Figures 6 and 7. We also tested the denoising performance of the proposed DLHPDE model on Peppers image with two levels of noise (variance = 0.002,0.005) and exhibited the results in Figures 8 and 9. As can been see from these results, the proposed method has better denoising performance. The quantitative comparison are outlined in Table 3. A very important discovery from the

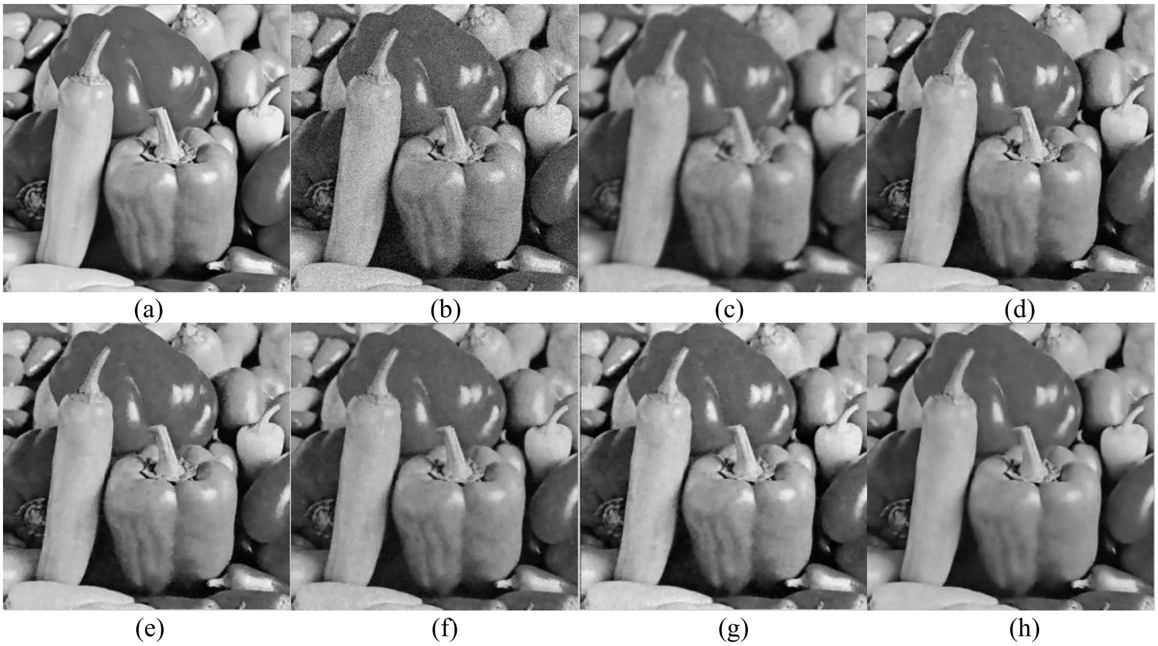

FIGURE 8. Comparison of denoising resultson Peppers image. (a) noise free image; (b) noisy image with variance of 0.002; Denoising results by (c) ID model, (d) PM model ($k = 6$), (e) VEPM model ($k = 4$), (f) MPM model, (g) TSP model ($k = 5$), as well as (h) DLHPDE model ($k = 2$).

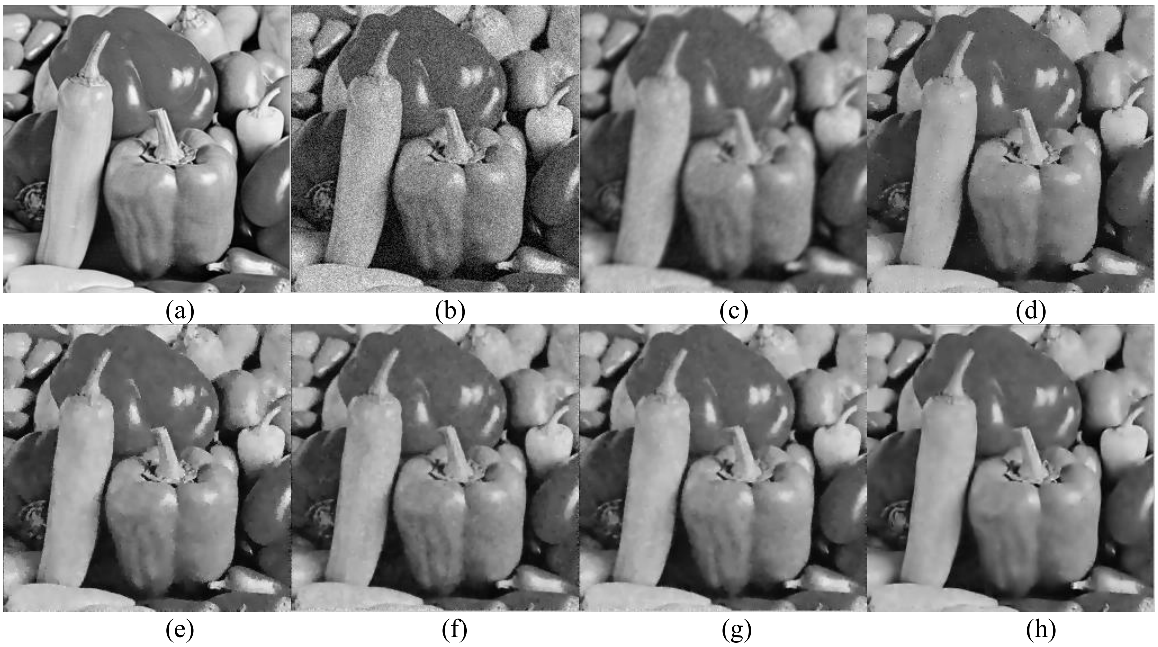

FIGURE 9. Comparison of denoising resultson Peppers image. (a) noise free image; (b) noisy image with variance of 0.005; Denoising results by (c) ID model, (d) PM model ($k = 6$), (e) VEPM model ($k = 4$), (f) MPM model, (g) TSP model ($k = 5$), as well as (h) DLHPDE model ($k = 2$).

Tables 1-3 is that our DLHPDE model generates the highest values of the PSNR, indicating that this proposed model has the best performance on removing noise while preserving the edges, textures, thin lines, weak edges and fine details. This method is also robust for different images with various levels of noise.

B. QUALITATIVE COMPARISON WITH SOME RECENT ADVANCED MODELS

In this subsection, we compared the proposed DLHPDE model with NLM model [54], BM3D model [55] and K-SVD model [56]. The test images include Straw (256×256) and Monarch (256×256). The two test

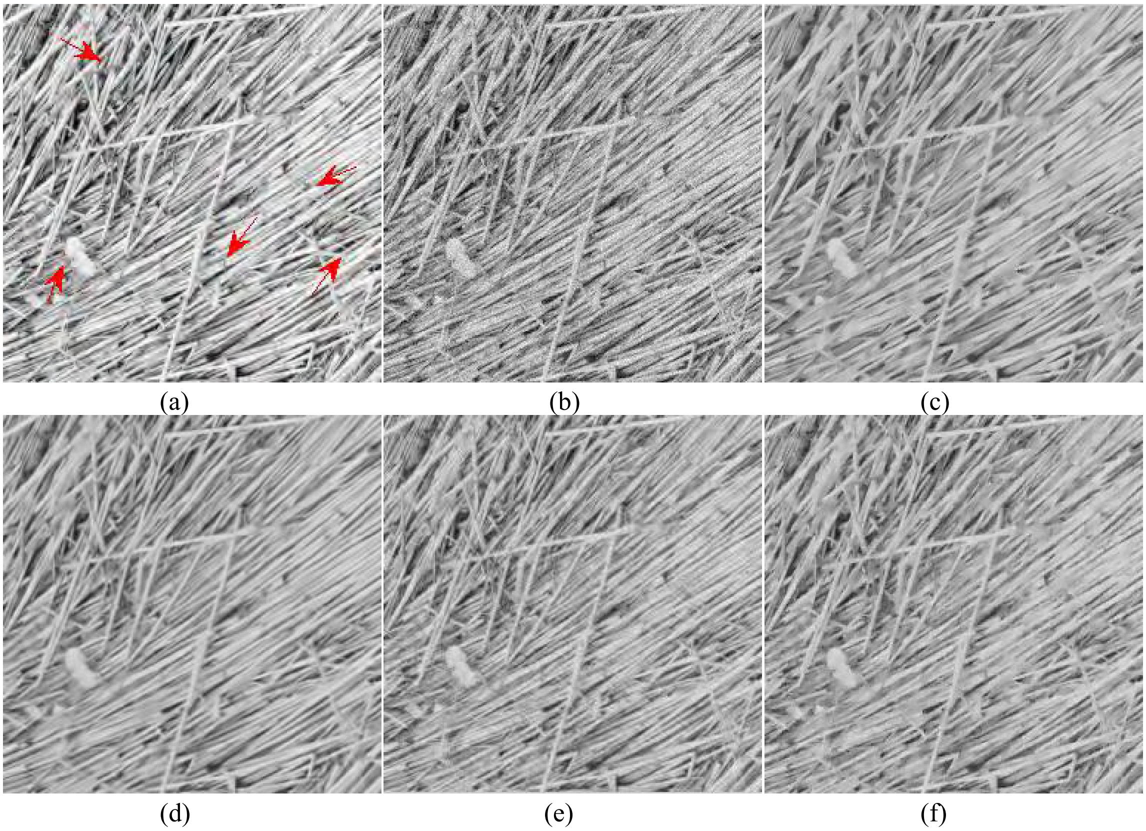

FIGURE 10. Comparison of denoising resultsonStraw image. (a) noise free image; (b) noisy image with variance of 0.002; Denoising results by (c) NLM model, (d) BM3D model, (e) K-SVD model, as well as (h) DLHPDE model ($k = 2$).

TABLE 3. Quantitative comparison of AGORITHMS IN DENOSING Peppers image

Model	Noise variance=0.002						Noise variance=0.005					
	ID	PM	VEPM	MPM	TSP	DLHPDE	ID	PM	VEPM	MPM	TSP	DLHPDE
PSNR	27.39	32.29	32.53	32.79	32.82	**33.41**	25.80	29.18	29.65	30.21	30.27	**30.77**

TABLE 4. Quantitative comparison of AGORITHMS IN DENOSING Straw image and Monarch image

Image	Straw		Monarch	
	PSNR	TIMES（S）	PSNR	TIMES(S)
NLM	27.56	4.62	29.64	4.14
BM3D	28.84	1.6	32.07	1.5
K-SVD	29.16	59.61	32.02	28.88
DLHPDE	28.81	3.61	**32.79**	2.97

images are corrupted by zero-mean Gaussian noise at variance of 0.002. The results on Straw image are listed in Figure 10 and those on the Monarch image are in Figure 11. The corresponding qualitative results and computing time are presented in Table 4. From Figure 10(c) and Figure 11(c), we observe that some edges and details of images are blurred severely (pointed by red arrows) in NLM model. As can been seen from Figures 10(d) and 11(d), BM3D has the best visual effects, the edges in BM3D are sharp even more than the noise free image. BM3D is a state-of-the-art denoising model that removes noise perfectly. But some fine details (pointed by red arrows) are filtered out in BM3D. Figure 10(e) and Figure 11(e) present KSVD model can preserve edges and fine details effectively, but the model consumes more time. Figure 10(f) and Figure 11(f) demonstrate that our proposed model preserves more details than other three models, which

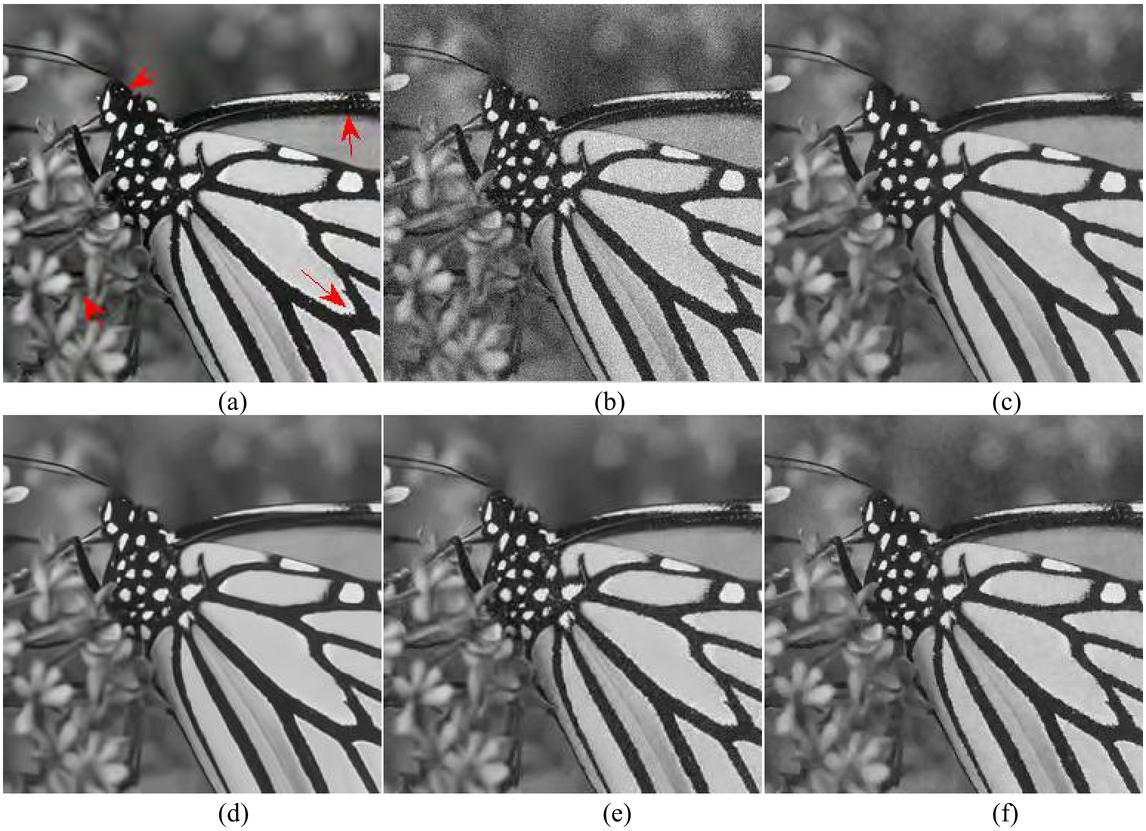

FIGURE 11. Comparison of denoising resultson Monarch image. (a) noise free image; (b) noisy image with variance of 0.002; Denoising results by (c) NLM model, (d) BM3D model, (e) K-SVD model, as well as (h) DLHPDE model ($k = 2$).

means the denoising results with our model are more similar to the true images. Those comparison results validate the fast convergence of the proposed model.

V. CONCLUTIONS

The aim of this article is to develop a hybrid denoising algorithm based on directional diffusion, via incorporating the advantage of the modified ID model and that of the modified PM model. In the proposed method, we employed the patch similarity modulus to serve as the structure indicator to control the diffusion mode and used the second order directional derivative to make the diffusion proceeds along the edge's direction of the original image. From comparison results, it can be seen that the proposed DLHPDE algorithm is more efficient to overcome the staircase effects, more clear to preserve thin lines, weak edges and fine details and more efficient to remove noise and aliasing around edges. To conclude, the visual and quantitative results have demonstrated that the quality of restored images by our method is better and more robust than the ID model, PM model, VEPM model, MPM model, and TSP model. We also compared our model with some recently advanced models, the experimental results demonstrated our proposed model has a better detail and texture preservation capability. To further validate the performance of the proposed DLHPDE model, our future efforts will be focused toward further optimizing the parameters of the proposed model such that it can be applied to the streak artifacts removal of the low-dose computed tomography (LDCT) images.

ACKNOWLEDGMENT

We would like to thank the anonymous reviewers for their valuable suggestions and constructive comments which improved the quality of this paper.

REFERENCES

[1] K. Panetta, L. Bao, and S. Agaian, "Sequence-to-sequence similarity-based filter for image denoising," *IEEE Sensors J.*, vol. 16, no. 11, pp. 4380–4388, Jun. 2016.
[2] J. Liu *et al.*, "3D feature constrained reconstruction for low-dose CT imaging," *IEEE Trans. Circuits Syst. Video Technol.*, vol. 28, no. 5, pp. 1232–1247, May 2018.
[3] W. Zhang, B. Ma, K. Liu, and R. Huang, "Video-based pedestrian re-identification by adaptive spatio-temporal appearance model," *IEEE Trans. Image Process.*, vol. 26, no. 4, pp. 2042–2054, Apr. 2017.
[4] Y. Chen *et al.*, "Artifact suppressed dictionary learning for low-dose CT image processing," *IEEE Trans. Med. Imag.*, vol. 33, no. 12, pp. 2271–2292, Dec. 2014.
[5] P. Chatterjee and P. Milanfar, "Is denoising dead?" *IEEE Trans. Image Process.*, vol. 19, no. 4, pp. 895–911, Apr. 2010.
[6] Y. Chen *et al.*, "Curve-like structure extraction using minimal path propagation with backtracking," *IEEE Trans. Image Process.*, vol. 25, no. 2, pp. 988–1003, Feb. 2016.

[7] Y. Chen, J. Ma, Q. Feng, L. Luo, P. Shi, and W. Chen, "Nonlocal prior Bayesian tomographic reconstruction," *J. Math. Imag. Vis.*, vol. 30, no. 2, pp. 133–146, 2008.

[8] A. P. Witkin, "Scale-space filtering," in *Proc. Int. Joint Conf. Artif. Intell.*, 1983, Karlsruhe, Germany, vol. 42, no. 3, pp. 1019–1022.

[9] P. Perona and J. Malik, "Scale-space and edge detection using anisotropic diffusion," *IEEE Trans. Pattern Anal. Mach. Intell.*, vol. 12, no. 7, pp. 629–639, Jul. 1990.

[10] L. I. Rudin, S. Osher, and E. Fatemi, "Nonlinear total variation based noise removal algorithms," *Phys. D, Nonlinear Phenomena*, vol. 60, nos. 1–4, pp. 259–268, 1992.

[11] A. N. Tikhonov and V. Y. Arsenin, "Solutions of ill-posed problem," *SIAM Rev.*, vol. 21, no. 2, pp. 266–267, 1979.

[12] F. Catté, P.-L. Lions, J.-M. Morel, and T. Coll, "Image selective smoothing and edge detection by nonlinear diffusion," *SIAM J. Numer. Anal.*, vol. 29, no. 1, pp. 182–193, 1992.

[13] Z. Guo, J. Sun, D. Zhang, and B. Wu, "Adaptive Perona–Malik model based on the variable exponent for image denoising," *IEEE Trans. Image Process.*, vol. 21, no. 3, pp. 958–967, Mar. 2012.

[14] Y. Q. Wang, J. Guo, W. Chen, and W. Zhang, "Image denoising using modified Perona–Malik model based on directional Laplacian," *Signal Process.*, vol. 93, no. 9, pp. 2548–2558, 2013.

[15] A. A. Yahya, J. Tan, and M. Hu, "A blending method based on partial differential equations for image denoising," *Multimedia Tools Appl.*, vol. 73, no. 3, pp. 1843–1862, 2014.

[16] J. Weickert, "Coherence-enhancing diffusion filtering," *Int. J. Comput. Vis.*, vol. 31, nos. 2–3, pp. 111–127, 1999.

[17] D. Tschumperlé and R. Deriche, "Vector-valued image regularization with PDEs: A common framework for different applications," *IEEE Trans. Pattern Anal. Machine Intell.*, vol. 27, no. 4, pp. 506–517, Apr. 2005.

[18] S. Mahmoodi, "Anisotropic diffusion for noise removal of band pass signals," *Signal Process.*, vol. 91, no. 5, pp. 1298–1307, 2011.

[19] M. R. Hajiaboli, "An anisotropic fourth-order diffusion filter for image noise removal," *Int. J. Comput. Vis.*, vol. 92, no. 2, pp. 177–191, 2011.

[20] M. Lysaker, A. Lundervold, and X.-C. Tai, "Noise removal using fourth-order partial differential equation with applications to medical magnetic resonance images in space and time," *IEEE Trans. Image Process.*, vol. 12, no. 12, pp. 1579–1590, Dec. 2003.

[21] Y.-L. You and M. Kaveh, "Fourth-order partial differential equations for noise removal," *IEEE Trans. Image Process.*, vol. 9, no. 10, pp. 1723–1730, Oct. 2000.

[22] M. R. Hajiaboli, "A self-governing hybrid model for noise removal," in *Advances in Image and Video Technology* (Lecture Notes in Computer Science), vol. 5414. Tokyo, Japan: Springer, 2009, pp. 295–305.

[23] T. Barbu, V. Barbu, V. Biga, and D. Coca, "A PDE variational approach to image denoising and restoration," *Nonlinear Anal., Real World Appl.*, vol. 10, no. 3, pp. 1351–1361, 2009.

[24] S.-M. Chao and D.-M. Tsai, "An improved anisotropic diffusion model for detail- and edge-preserving smoothing," *Pattern Recognit. Lett.*, vol. 31, no. 13, pp. 2012–2023, 2010.

[25] V. B. S. Prasath and D. Vorotnikov, "Weighted and well-balanced anisotropic diffusion scheme for image denoising and restoration," *Nonlinear Anal., Real World Appl.*, vol. 17, pp. 33–46, Jun. 2013.

[26] J. Xu, Y. Jia, Z. Shi, and K. Pang, "An improved anisotropic diffusion filter with semi-adaptive threshold for edge preservation," *Signal Process.*, vol. 119, pp. 80–91, Feb. 2016.

[27] A. A. Yahya and J. Tan, "A novel partial differential equation method based on image features and its applications in denoising," in *Proc. 4th IEEE Int. Conf. Digit. Home*, Guangzhou, China, Nov. 2012, pp. 46–51.

[28] X. W. Liu, "Efficient algorithms for hybrid regularizers based image denoising and deblurring," *Comput. Math. Appl.*, vol. 69, no. 7, pp. 675–687, 2015.

[29] T. Barbu, "PDE-based restoration model using nonlinear second and fourth order diffusions," *Proc. Romanian Acad., A*, vol. 16, no. 2, pp. 138–146, 2015.

[30] S. Kim, "PDE-based image restoration: A hybrid model and color image denoising," *IEEE Trans. Image Process.*, vol. 15, no. 5, pp. 1163–1170, May 2006.

[31] T. Barbu, "Compound PDE-based image restoration algorithm using second-order and fourth-order diffusions," in *Neural Information Processing*. Tokyo, Japan: Springer, 2016, pp. 699–706.

[32] V. B. S. Prasath and A. Singh, "A hybrid convex variational model for image restoration," *Appl. Math. Comput.*, vol. 215, no. 10, pp. 3655–3664, 2010.

[33] P. Kornprobst, R. Deriche, and G. Aubert, "Nonlinear operators in image restoration," in *Proc. Comput. Vis. Pattern Recognit.*, Jun. 1997, pp. 325–331.

[34] G. Sapiro and D. L. Ringach, "Anisotropic diffusion of multivalued images with applications to color filtering," *IEEE Trans. Image Process.*, vol. 5, no. 11, pp. 1582–1586, Nov. 1996.

[35] Y.-L. You, W. Xu, A. Tannenbaum, and M. Kaveh, "Behavioral analysis of anisotropic diffusion in image processing," *IEEE Trans. Image Process.*, vol. 5, no. 11, pp. 1539–1553, Nov. 1996.

[36] D. Tschumperlé and R. Deriche, "Diffusion PDEs on vector-valued images," *IEEE Signal Process. Mag.*, vol. 19, no. 5, pp. 16–25, Sep. 2002.

[37] D. Tschumperlé and R. Deriche, "Anisotropic diffusion partial differential equations in multi-channel image processing: Framework and applications," *Adv. Imag. Electron Phys.*, vol. 145, pp. 149–209, Jan. 2007.

[38] D. Ziou and A. Horé, "Reducing aliasing in images: A PDE-based diffusion revisited," *Pattern Recognit.*, vol. 45, no. 3, pp. 1180–1194, 2012.

[39] Y. Wang, W. Chen, S. Zhou, T. Yu, and Y. Zhang, "MTV: Modified total variation model for image noise removal," *Electron. Lett.*, vol. 47, no. 10, pp. 592–594, May 2011.

[40] Y. Wang, W. Ren, and H. Wang, "Anisotropic second and fourth order diffusion models based on convolutional virtual electric field for image denoising," *Comput. Math. Appl.*, vol. 66, no. 10, pp. 1729–1742, 2013.

[41] C. Tsiotsios and M. Petrou, "On the choice of the parameters for anisotropic diffusion in image processing," *Pattern Recognit.*, vol. 46, no. 5, pp. 1369–1381, 2013.

[42] K. Liu, J. Tan, and L. Ai, "Hybrid regularizers-based adaptive anisotropic diffusion for image denoising," *SpringerPlus*, vol. 5, p. 404, Dec. 2016.

[43] Y. Xu and J. Yuan, "Anisotropic diffusion equation with a new diffusion coefficient for image denoising," *Pattern Anal. Appl.*, vol. 20, no. 2, pp. 579–586, 2017.

[44] M. B. Abdallah *et al.*, "Adaptive noise-reducing anisotropic diffusion filter," *Neural Comput. Appl.*, vol. 27, no. 5, pp. 1273–1300, 2016.

[45] P. Jain and V. Tyagi, "An adaptive edge-preserving image denoising technique using tetrolet transforms," *Vis. Comput.*, vol. 31, no. 5, pp. 657–674, 2015.

[46] W. Zhang and W.-K. Cham, "Hallucinating face in the DCT domain," *IEEE Trans. Image Process.*, vol. 20, no. 10, pp. 2769–2779, Oct. 2011.

[47] Q. Chen, Y. Zheng, Q. Sun, and D. Xia, "Patch similarity based anisotropic diffusion for image denoising," *J. Comput. Res. Develop.*, vol. 47, no. 1, pp. 33–42, 2010.

[48] Y. Chen *et al.*, "Structure-adaptive fuzzy estimation for random-valued impulse noise suppression," *IEEE Trans. Circuits Syst. Video Technol.*, vol. 28, no. 2, pp. 414–427, Feb. 2018.

[49] J. Liu *et al.*, "Discriminative feature representation to improve projection data inconsistency for low dose CT imaging," *IEEE Trans. Med. Imag.*, vol. 36, no. 12, pp. 2499–2509, Dec. 2017.

[50] W. Zhang and W.-K. Cham, "Gradient-directed multiexposure composition," *IEEE Trans. Image Process.*, vol. 21, no. 4, pp. 2318–2323, Apr. 2012.

[51] W. Zhang, C. Qu, L. Ma, J. Guan, and R. Huang, "Learning structure of stereoscopic image for no-reference quality assessment with convolutional neural network," *Pattern Recognit.*, vol. 59, pp. 176–187, Nov. 2016.

[52] Z. Wang, A. C. Bovik, H. R. Sheikh, and E. P. Simoncelli, "Image quality assessment: From error visibility to structural similarity," *IEEE Trans. Image Process.*, vol. 13, no. 4, pp. 600–612, Apr. 2004.

[53] A. Horé and D. Ziou, "Is there a relationship between peak-signal-to-noise ratio and structural similarity index measure?" *IET Image Process.*, vol. 7, no. 1, pp. 12–24, Feb. 2013.

[54] A. Buades, B. Coll, and J.-M. Morel, "A non-local algorithm for image denoising," in *Proc. IEEE Comput. Soc. Conf. Comput. Vis. Pattern Recognit.*, vol. 2. San Diego, CA, USA, Jun. 2005, pp. 60–65.

[55] K. Dabov, A. Foi, V. Katkovnik, and K. Egiazarian, "Image denoising by sparse 3D transform-domain collaborative filtering," *IEEE Trans. Image Process.*, vol. 16, no. 8, pp. 2080–2095, Aug. 2007.

[56] M. Elad and M. Aharon, "Image denoising via sparse and redundant representations over learned dictionaries," *IEEE Trans. Image Process.*, vol. 15, no. 12, pp. 3736–3745, Dec. 2006.

NA WANG received the M.S. degree in signal and information processing from the North University of China, Taiyuan, China, in 2015, where she is currently pursuing the Ph.D. degree. Her research interests include image denoising and enhancement.

YU SHANG received the B.S. degree in applied mathematics and the M.S. degree in biomedical engineering from Jilin University, China, in 1999 and 2004, respectively, and the Ph.D. degree in biomedical engineering from Tsinghua University, China, in 2008. From 2008 to 2013, he was a Post-Doctoral Scholar/Fellow with the University of Kentucky, USA, where he was a Research Scientist from 2013 to 2015. He is currently a Full Professor with the North University of China. His research interests include image reconstruction, biomedical optical spectroscopy, and tomography.

YANG CHEN received the M.S. and Ph.D. degrees in biomedical engineering from First Military Medical University, China, in 2004 and 2007, respectively. Since 2008, he has been a Faculty Member with the Department of Computer Science and Engineering, Southeast University, China. His recent work concentrates on the medical image reconstruction, image analysis, pattern recognition, and computerized-aid diagnosis.

MIN YANG received the Ph.D. degree from the School of Mechanical Engineering and Automation, Beijing University of Aeronautics and Astronautics (BUAA), in 2004. He is currently a Professor with BUAA. His research interests mainly include multidimensional information reconstruction and recognition, X-ray digital radiography, CT theory, and application.

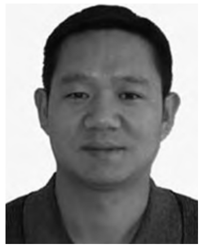

QUAN ZHANG received the Ph.D. degree in computer science and technology from Southeast University, Nanjing, China, in 2015. He is currently with the North University of China, where he is involved in teaching and research. His research interests include medical image reconstruction and medical image analysis.

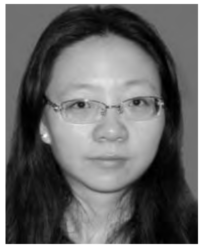

YI LIU received the Ph.D. degree in signal and information processing from the North University of China in 2014. She was a Post-Doctoral Scholar with the Université de Rennes 1 from 2014 to 2015. She joined the School of Information and Communication Engineering, North University of China, in 2015. Her research interests include CT reconstruction and image processing.

ZHIGUO GUI received the Ph.D. degree in signal and information processing from the North University of China in 2004. He was a Post-Doctoral Researcher with Southeast University, China. He is currently a Full Professor with the North University of China. His research interests include image processing and image reconstruction.